Eur. Phys. J. B **34**, 429–440 (2003)
DOI: 10.1140/epjb/e2003-00241-1

THE EUROPEAN PHYSICAL JOURNAL B

Point-defect properties in HCP rare earth metals with analytic modified embedded atom potentials

Wangyu Hu[1,2,a], Huiqiu Deng[1], Xiaojian Yuan[1], and Masahiro Fukumoto[2]

[1] Department of Applied Physics, Hunan University, Changsha, 410082, PR China
[2] Department of Production Systems Engineering, Toyohashi University of Technology, 1-1, Tempaku-cho, Toyohashi, 441-8580 Japan

Received 6 January 2002 / Received in final form 26 March 2003
Published online 9 September 2003 –

Abstract. The analytic embedded atom method (EAM) type many-body potentials of hcp rare earth metals (Dy, Er, Gd, Ho, Nd, Pr, and Tb) have been constructed. The hcp lattice is shown to be energetically most stable when compared with the fcc and bcc structure, and the hcp lattice with ideal c/a. The mechanical stability of the corresponding hcp lattice with respect to large change of density and c/a ratio is examined. The phonon spectra, stacking fault and surface energy are calculated. The activation energy for vacancy diffusion in these metals has been calculated and the most possible diffusion paths are predicted. Finally, the self-interstitial atom (SIA) formation energy and volume have been evaluated for eight possible sites. This calculation suggests that the crowdion and basal split are the most stable configurations. The SIA formation energy increases linearly with the increase of the melting temperature.

PACS. 34.20.Cf Interatomic potentials and forces – 66.30.Fq Self-diffusion in metals, semimetals, and alloys – 61.72.Ji Point defects (vacancies, interstitials, color centers, etc.) and defect clusters – 61.72.Bb Theories and models of crystal defects

1 Introduction

Since 1794, the year of Johan Gadolin's discovery of yttrium, rare earth materials have contributed to the improvement of civilization. The rare earths were once scientific curiosities, but modern methods of separation and new applications, particularly in the fields of atomic energy and metals research, make them commercially valuable. Rare earths are used as catalysts in automotive catalytic converters, as iron and steel additives, as ceramic and glass additives for their decolorizing properties, as light-emitting substances (phosphors), and as components in electronic devices, permanent magnets, light bulbs, and in various aspects of research. Rare earths are expected to play an important role in advanced materials, which are essential for industrially high quality and high performance products. One of the basic concepts to understand the superb performance of these materials is the atomistic interaction of the rare earth metals. It is the basis for computer simulation of defects and prediction of their properties. The reliability of the atomistic simulations depends on the accuracy of the modeled atomic interactions. While first-principles methods constitute the most reliable approach to determining atomic interactions, application of these methods to systems with more than a few hundred atoms is not feasible. Most atomistic simulations of defects in metals are performed using semiempirical or empirical descriptions of atomic interactions. Only a few *ab initio* studies have been devoted to defects in metals or alloys. Domain and Becquart [1] have reported the *ab initio* calculations of defects in Fe and dilute Fe-Cu alloys. Han *et al.* [2,3] have studied the self-interstitials and vacancies in V and Mo with an extensive ab initio calculations recently.

Properties of hcp metals have occasionally been calculated using empirical pair potential interactions, but application to hcp metals is less common than to cubic metals [4,5]. Recently, many-body potentials have been developed for hcp metals [6–13]. The potentials proposed by Igarashi *et al.* [6] for the eight metals, Be, Hf, Ti, Ru, Zr, Co, Mg, Zn were fitted to several physical parameters, including the c/a ratio, but not to any data that arise from atom-atom interactions inside the normal equilibrium lattice spacing. The extreme hard pair repulsion term leads to very large values of interstitial atom formation energy. Moreover, Bacon found that some the potentials produce an unstable crystal when used to model twin boundaries [5]. The modified EAM potentials proposed by Baskes and Johnson [7] with angular forces were applied to eighteen hcp metals, including hcp rare-earth metals. They studied the vacancy, divacancy, stacking fault

[a] e-mail: wangyuhu2001cn@yahoo.com.cn, wyuhu@hnu.cn

and surface, but the divacancy was unbound in all of the metals considered except Be. Moreover, no information was given about the application of their model to self-interstitial atoms. The many-body potentials for hcp metals proposed by Johnson *et al.* [8–10] and Ackland [11,12] are only appropriate for metals such as Mg, Ti, and Zr, which have a c/a lattice parameter ratio close to the ideal value.

Based on these work, we have constructed new analytic modified EAM many-body potentials for hcp metals currently, and calculated the thermodynamic properties of Mg-RE alloys [13,14]. These potentials reproduce exactly the observed c/a ratio and all five elastic constants for each metal considered, and guarantee the stability of the hexagonal structure with respect to hcp with ideal c/a, fcc, and bcc crystal structures. The formation and migration energies of the vacancy, the activation energy for self-diffusion of monovacancy, the divacancy formation and binding energies, and the activation energy for diffusion by a divacancy mechanism, stacking fault and surface energies, and the self-interstitial atom (SIA) formation energy have been calculated. These calculations agree well with the experimental data available. In the present paper, these potentials are applied for hcp rare earth metals and properties of various defects are evaluated.

2 Determination of the potential parameters

Due to the fundamental invariance of physical space under continuous translations or rotations, corresponding to the homogeneity and isotropy of space, the potential energy must be invariant under any change of the origin of the coordinates or under any rotation of the coordinates axes. However, in the previous paper [13,14], the interaction model is not invariant under these rotations. We have improved the potentials in the present paper.

As described previously, parameters should be introduced to correct the Cauchy relations, and the number of parameters should be the same as the Cauchy relations for the specific crystal. Moreover, this number is also related to crystal symmetry, *i.e.*, the number of independent parameters of symmetry operation for the seven crystal systems. There are 6 parameters for triclinic, 4 for monoclinic, 3 for orthorhombic, 2 for tetragonal, trigonal, and hexagonal, and 1 for cubic. In the present model, the number of modification terms is the same as the Cauchy relations, each term only has one parameter, to ensure the invariance of the potential. The arguments of the modification terms are the sum of high orders of electron density to correct the discrepancy of the linear superposition of atomic electron density.

The physical properties fitted within this scheme are the cohesive energy, E_c, vacancy formation energy, E_{1f}, five independent second-order elastic constants, and the two lattice constants of the hexagonal structure, a and c. All these quantities are summarized in Table 1.

In this scheme, the basic equation of the total energy of a system of atoms is

$$E_t = \sum E_i \tag{1}$$

where the contribution from the atom at site i is

$$E_i = F(\rho_i) + \frac{1}{2}\sum_j \phi(r_{ij}) + M(P_i) + N(Q_i) \tag{2}$$

The energy modification terms are empirically taken as

$$M(P_i) = \alpha\left\{1 - \exp\left[-10000\left(\ln\left(\frac{P_i}{P_e}\right)\right)^2\right]\right\} \tag{3}$$

$$N(Q_i) = \beta\left\{1 - \exp\left[-10000\left(\ln\left(\frac{Q_i}{Q_e}\right)\right)^2\right]\right\} \tag{4}$$

where P_e and Q_e are their equilibrium values. The host electron density is taken in the original form

$$\rho_i = \sum_j f(r_{ij}) \tag{5}$$

and the arguments of the energy modification terms are taken as

$$P_i = \sum_j f^2(r_{ij}) \tag{6}$$

$$Q_i = \sum_j f^3(r_{ij}) \tag{7}$$

In the present paper, only one electron density function is used [15], it is defined as

$$f(r_{ij}) = f_e\left(\frac{r_1}{r_{ij}}\right)^{4.5}\left(\frac{r_{ce} - r_{ij}}{r_{ce} - r_1}\right)^2 \tag{8}$$

where the parameter f_e is taken as 1 as was done by Johnson [9]. $f(r)$ is truncated at r_{ce}, $r_{ce} = r_8 + k_c(r_9 - r_8)$, r_8 and r_9 are the 8th and 9th nearest neighbor distance for a perfect hcp crystal with its actual c/a ratio respectively, k_c is another adjustable parameter, which ensures no oscillation in the pair potential and the crystal stability, and it is listed in Table 2. $f(r)$ is 0 if r is larger than r_{ce}.

The embedding function $F(\rho_i)$ takes the same form as those used by Johnson and Oh [8]:

$$F(\rho_i) = -F_0\left[1 - n\ln\left(\frac{\rho_i}{\rho_e}\right)\right]\left(\frac{\rho_i}{\rho_e}\right)^n \tag{9}$$

where $F_0 = E_c - E_{1f}$. ρ_e takes its equilibrium value. n is an adjustable parameter and its specific value for each element is determined by fitting the empirical energy-volume relationship of Rose *et al.* [20], which ensures reasonable response for atomic spacing just inside the first-neighbour distance.

Table 1. Quantities used in the fitting of the potentials. Values of a and c have been taken from Barrett and Massalski [16], values of E_c from Kittel [17] and vacancy formation energies E_{1f} from Baskes and Johnson [7], E_{1f} of Pr and Nd from de Boer *et al.* [18]. Values of elastic constants from Brands [19]. a and c are in nm, E_c and E_{1f} in eV and C_{ij} in GPa.

	Dy	Er	Gd	Ho	Nd	Pr	Tb
a	0.35923	0.35590	0.36315	0.35761	0.36582	0.36702	0.35990
c	0.56545	0.55920	0.57770	0.56174	0.59010	0.59140	0.56960
E_c	3.04	3.29	4.14	3.14	3.40	3.70	4.05
E_{1f}	1.22	1.32	1.13	1.27	1.24	1.24	1.18
C_{11}	74.0	84.1	66.7	76.5	54.8	49.4	69.2
C_{12}	25.5	29.4	25.0	25.6	24.6	23.0	25.0
C_{44}	24.3	27.4	20.7	25.9	15.0	13.6	21.8
C_{13}	21.8	22.6	21.3	21.0	16.6	14.3	21.8
C_{33}	78.6	84.7	71.9	79.6	60.9	57.4	74.4

Table 2. Parameters of the many-body potentials for hcp metals. n is in dimensionless, F_0, α, β and k_i are in eV.

	Dy	Er	Gd	Ho	Nd	Pr	Tb
n	0.49	0.49	0.45	0.49	0.45	0.38	0.45
F_0	1.82	1.97	3.01	1.87	2.16	2.46	2.87
$\alpha \times 10^6$	8.37331	22.1373	14.6398	11.1886	126.680	128.990	5.0892
$\beta \times 10^6$	−6.7179	−13.430	−9.752	−8.5469	−57.981	−58.676	−5.541
k_c	0.45	0.55	0.35	0.45	0.45	0.10	0.40
k_{-1}	280.324	244.563	342.200	280.600	221.838	117.928	308.480
k_0	−1361.7	−1175.1	−1670.6	−1364.1	−1067.8	−548.78	−1503.8
k_1	2819.08	2410.12	3467.05	2827.28	2187.76	1091.81	3120.27
k_2	−3226.2	−2738.4	−3966.6	−3240.9	−2475.0	−1207.0	−3573.4
k_3	2203.04	1860.29	2701.19	2217.52	1668.49	800.211	2438.32
k_4	−896.77	−754.75	−1094.3	−904.70	−669.62	−317.50	−990.61
k_5	201.307	169.121	244.144	203.565	148.014	69.6499	221.738
k_6	−19.211	−16.129	−23.133	−19.472	−13.894	−6.5043	−21.088

The pair potential is taken as:

$$\phi(r_{ij}) = \sum_{m=-1}^{m=6} k_m \left(\frac{r_{ij}}{r_1}\right)^m \tag{10}$$

The atomic interactions out to the seventh neighbor distance are considered and it is truncated at a specific cutoff distance $r_c = r_7 + k_c(r_8 - r_7)$.

As a similar way, the model parameters, α, β, n, and $k_m (m = -1, 0, 1, 2, 3, 4, 5, 6)$ have been determined and listed in Table 2.

All of the pair potentials and embedding functions for these metals are shown in Figures 1 and 2, respectively. A distinct minimum near the nearest neighbor distance can be found. The values of the modification functions are equal to zero at r_1 and are very small for the other atomic distance as shown in Figure 3 for Tb. All the modification terms M(P) are positive, and N(Q) are negative, because they have one or two negative Cauchy pressures. Figure 4 shows the comparison of the curve of total energy for the present model with that from the Rose equation [20].

3 Results and discussion

3.1 Structural and mechanical stability

The lattice stability of the particular hcp structure relative to the hcp structure with ideal c/a ratio, fcc and bcc crystal structures are predicted and shown in Figure 5, and the structural energy differences at equilibrium volume are listed in Table 3. The predictions from the modified embedded atom potentials of Baskes and Johnson [7] (B-J potentials) are also included in the same table as comparison. The structural energy difference is very small

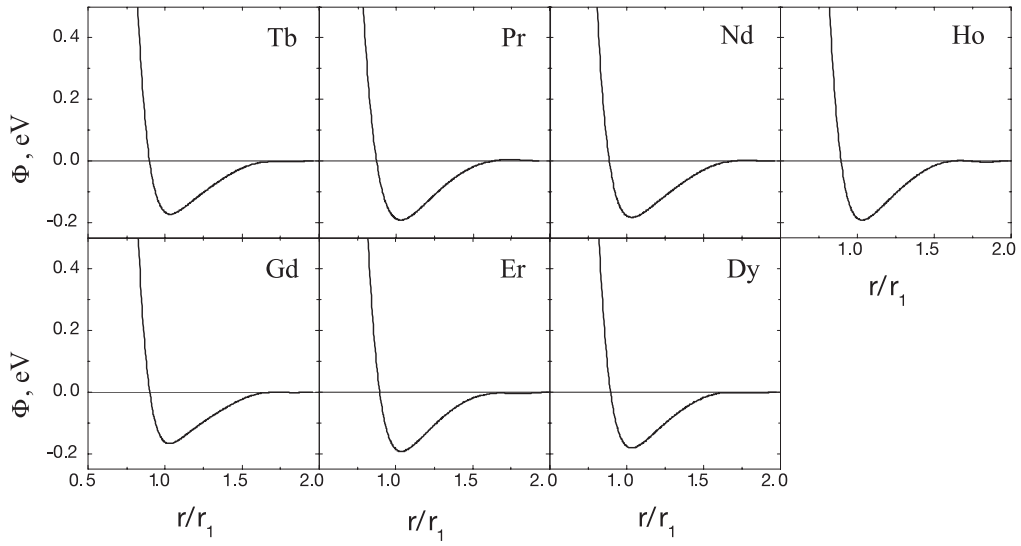

Fig. 1. Potentials for Dy, Er, Gd, Ho, Nd, Pr and Tb.

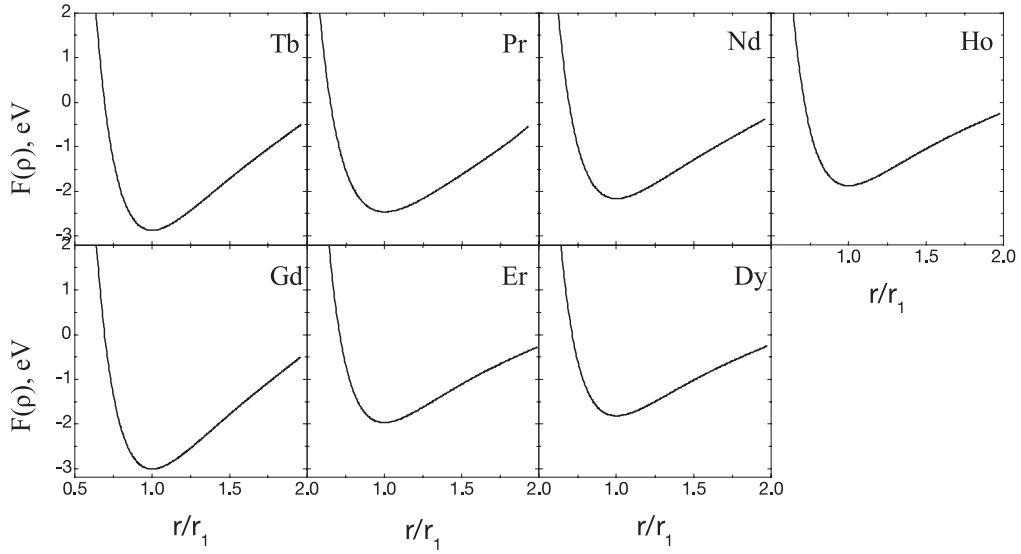

Fig. 2. Embedding functions for Dy, Er, Gd, Ho, Nd, Pr and Tb.

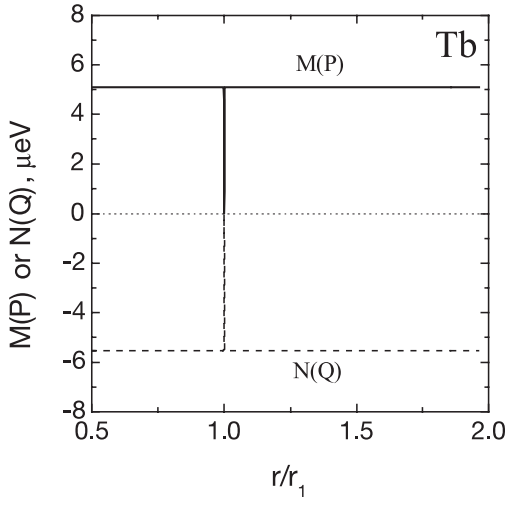

Fig. 3. Energy modification terms for Tb.

(0.0002 eV) for Pr and Nd, whose c/a ratios are 1.611 and 1.613, respectively. It increases with decreasing c/a ratio, up to 0.0019 eV for Er, whose c/a ratio is 1.571. Figure 6 shows the relation between the structural energy difference $(E_{\mathrm{hcp,\,ideal\,c/a}} - E_{\mathrm{hcp}})/E_c$ and (1.633-c/a) for the metals considered. The squares represent the present calculations and the dash line is the fitting result for these points. The solid circles are the calculated results of Baskes and Johnson [7]. From this figure, it can be seen that the structural energy difference increases nonlinearly with the difference between ideal c/a and real c/a as described in the previous paper [14]. The structural stability of the close packed hexagonal lattice relative to fcc and bcc is also shown in Table 3, although the structural energy difference is small as comparing with those from B-J potentials [4], and it gives the same result that the fitted hcp lattice is indeed the most stable one.

$$
\begin{aligned}
\Phi_{\alpha\beta}(\boldsymbol{r}_{ij}) =& \frac{r_{ij\alpha}r_{ij\beta}}{r_{ij}^2}\left[\Phi''(r_{ij}) - \frac{\Phi'(r_{ij})}{r_{ij}}\right] + \delta_{\alpha\beta}\frac{\Phi'(r_{ij})}{r_{ij}} + \sum_{k\neq i,j} F''(\rho_k)f'(r_{jk})f'(r_{ik})\frac{r_{jk\beta}r_{ik\alpha}}{r_{ij}^2} \\
&+ \big[F'(\rho_i) + F'(\rho_j)\big]\left\{\frac{r_{ij\beta}r_{ij\alpha}}{r_{ij}^2}\left[f''(r_{ij}) - \frac{f'(r_{ij})}{r_{ij}}\right] + \delta_{\alpha\beta}\frac{f'(r_{ij})}{r_{ij}}\right\} \\
&- F''(\rho_i)f'(r_{ij})\frac{r_{ij\beta}}{r_{ij}}\sum_{k\neq i} f'(r_{ik})\frac{r_{ik\alpha}}{r_{ik}} - F''(\rho_j)f'(r_{ij})\frac{r_{ij\alpha}}{r_{ij}}\sum_{k\neq j} f'(r_{jk})\frac{r_{jk\beta}}{r_{jk}} \\
&+ 4\sum_{k\neq i,j} M''(p_k)f(r_{jk})f'(r_{jk})f(r_{ik})f'(r_{ik})\frac{r_{jk\beta}r_{ik\alpha}}{r_{ik}^2} \\
&+ 2\big[M'(p_i) + M'(p_j)\big]\left\{\frac{r_{ij\beta}r_{ij\alpha}}{r_{ij}^2}\left[f(r_{ij})f''(r_{ij}) + (f'(r_{ij}))^2 - \frac{f(r_{ij})f'(r_{ij})}{r_{ij}}\right] + \delta_{\alpha\beta}\frac{f(r_{ij})f'(r_{ij})}{r_{ij}}\right\} \\
&- 4M''(p_i)f(r_{ij})f'(r_{ij})\frac{r_{ij\beta}}{r_{ij}}\sum_{k\neq i} f(r_{ik})f'(r_{ik})\frac{r_{ik\alpha}}{r_{ik}} \\
&- 4M''(p_j)f(r_{ij})f'(r_{ij})\frac{r_{ij\alpha}}{r_{ij}}\sum_{k\neq j} f(r_{jk})f'(r_{jk})\frac{r_{jk\beta}}{r_{jk}} \\
&+ 9\sum_{k\neq i,j} N''(q_k)f^2(r_{jk})f'(r_{jk})f^2(r_{ik})f'(r_{ik})\frac{r_{jk\beta}r_{ik\alpha}}{r_{ij}^2} \\
&+ 3\big[N'(q_i) + N'(q_j)\big]\left\{\frac{r_{ij\beta}r_{ij\alpha}}{r_{ij}^2}\left[f^2(r_{ij})f''(r_{ij}) + 2f(r_{ij})\big(f'(r_{ij})\big)^2 - \frac{f^2(r_{ij})f'(r_{ij})}{r_{ij}}\right] + \delta_{\alpha\beta}\frac{f^2(r_{ij})f'(r_{ij})}{r_{ij}}\right\} \\
&- 9N''(q_i)f^2(r_{ij})f'(r_{ij})\frac{r_{ij\beta}}{r_{ij}}\sum_{k\neq i} f^2(r_{ik})f'(r_{ik})\frac{r_{ik\alpha}}{r_{ik}} \\
&- 9N''(q_j)f^2(r_{ij})f'(r_{ij})\frac{r_{ij\alpha}}{r_{ij}}\sum_{k\neq j} f^2(r_{jk})f'(r_{jk})\frac{r_{jk\beta}}{r_{jk}}. \qquad (11)
\end{aligned}
$$

The mechanical stability of the hcp lattice with respect to large homogeneous expansions and compressions has been tested by calculating the energy of the hcp crystal for different values of the atomic volume and c/a ratio. The dependence of cohesive energy on c/a ratio at different values of atomic volume for Dy is shown in Figure 7. It is seen that in this range of the c/a values and volume changes, no other hcp metastable configurations exist under the constructed potential. Moreover, the c/a ratio corresponding to the lowest energy structure increases with decreasing atomic volume, that is, with increasing compression, and converges towards the ideal value, 1.633. Clearly, under high compression the atoms tend to behave like hard spheres owing to strong repulsion. The same results have been found for all the potentials constructed.

3.2 Phonon dispersion curves

The potential's ability to predict phonon dispersion curves is considered to be a useful test because phonon dispersion curves can be measured experimentally. The hcp metals posses lower symmetry than the metals of the fcc and bcc phases. Therefore, it is comparatively difficult to study the lattice dynamics of hcp crystals using many-body potentials or first-principle methods. Until recently, using FS many-body potentials, Igarashi *et al.* [6] calculated the phonon dispersion relations of eight hexagonal metals (Co, Zr, Ti, Ru, Hf, Zn, Mg and Be). However, there are some mistakes in their expressions of the dynamical matrix and force constants as shown below. Another approach was the calculations of phonon spectra of Sc, Y, Tb, Ho and Lu with the rare earth metal pair potential by Singh [21].

Using the Born-von Karman lattice dynamics [22] and the present potentials, the force constants are:

see equation (11) above

In the paper of Igarashi *et al.* [6], the dynamical matrix of equation (11) was incomplete when $\lambda = \lambda'$. Similarly, equation (12) in their paper for the force constant was also incomplete in the last term for the second derivation of the embedding function, two terms (for $k \neq i$ and $k \neq j$) were lost. However, in their actual calculations, the first problem in equation (11) is corrected, the lost terms in equation (12) are not considered.

Phonon spectra were calculated using the constructed potentials for the wave-vectors parallel to three high symmetry directions, [001], [100] and [110], in the Brillouin zone of the hexagonal lattice. The results, together with available experimental data, are shown in Figure 8. The experimental data are available only for Tb and Ho. The calculated curves do capture important experimental features, and there is in good agreement with experimental data for these two elements, which indicates that the present potentials display reasonable lattice dynamics behavior.

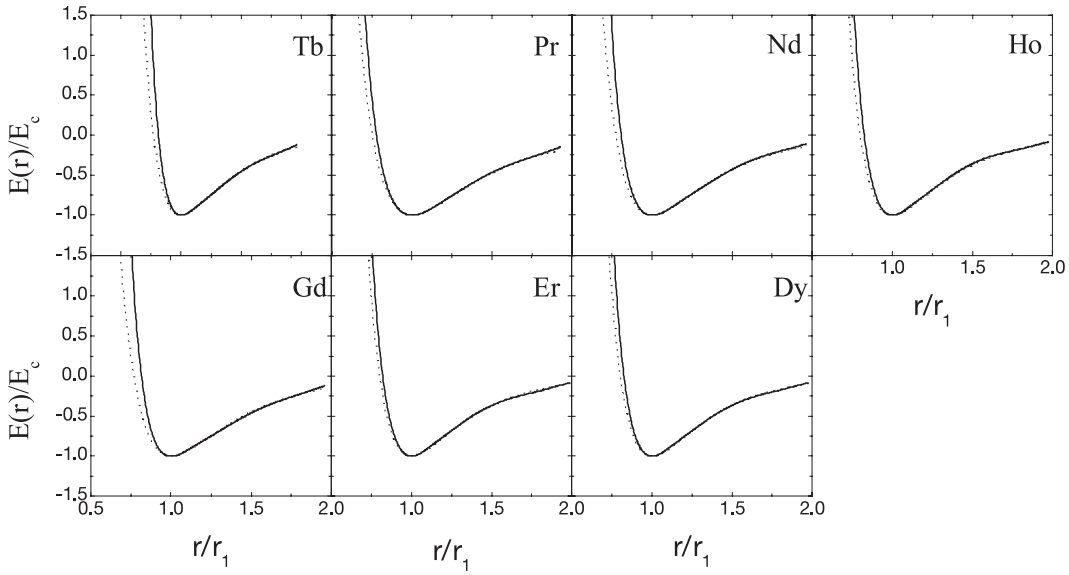

Fig. 4. The total energies as a function of r/r_1 for hcp rare earth metals. The solid curves are the results calculated from the present potentials; the dashed curves are the results from the Rose equation.

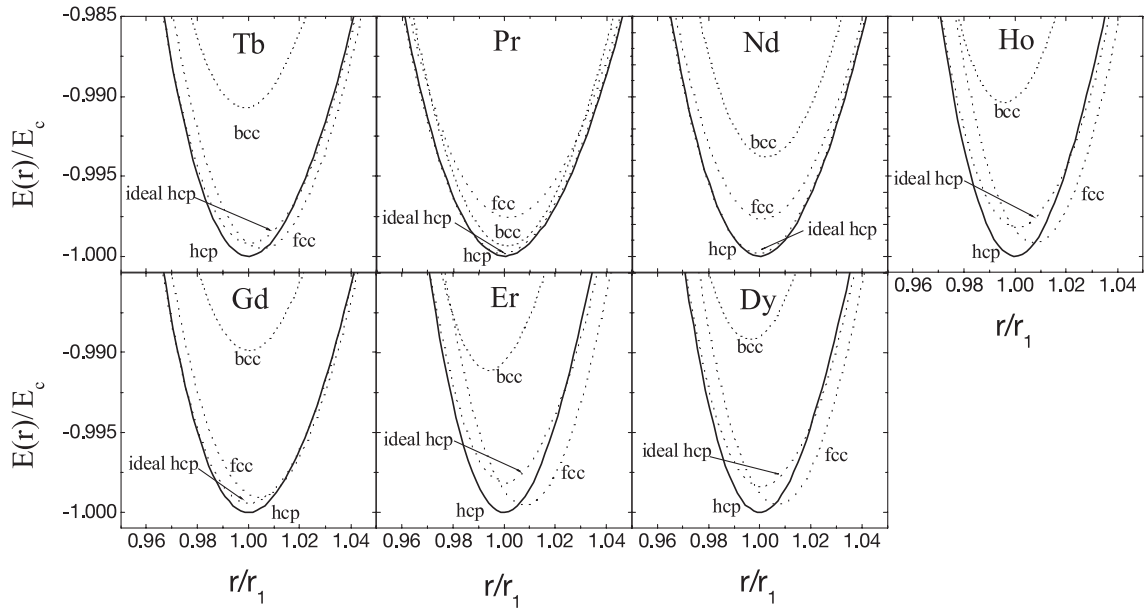

Fig. 5. Lattice stability of hcp, fcc, bcc, and ideal c/a ratio hcp structures.

Table 3. Calculated values of lattice stabilities for hcp with ideal c/a ratio, fcc, and bcc crystal structures relative to the real hcp structure (in eV/atom).

Element		Dy	Er	Gd	Ho	Nd	Pr	Tb
HCP	Present	0.0016	0.0019	0.0006	0.0018	0.0002	0.0002	0.0008
(ideal c/a)	B-J [7]	0.0065	0.0055	0.0019	0.0054	0.0003	0.0001	0.0023
FCC	Present	0.0012	0.0013	0.0011	0.0017	0.0023	0.0024	0.0007
	B-J [7]	0.057	0.054	0.029	0.053	0.012	0.008	0.031
BCC	Present	0.0110	0.0095	0.0101	0.0098	0.0063	0.0006	0.0093
	B-J [7]	0.190	0.207	0.265	0.196	0.211	0.210	0.247

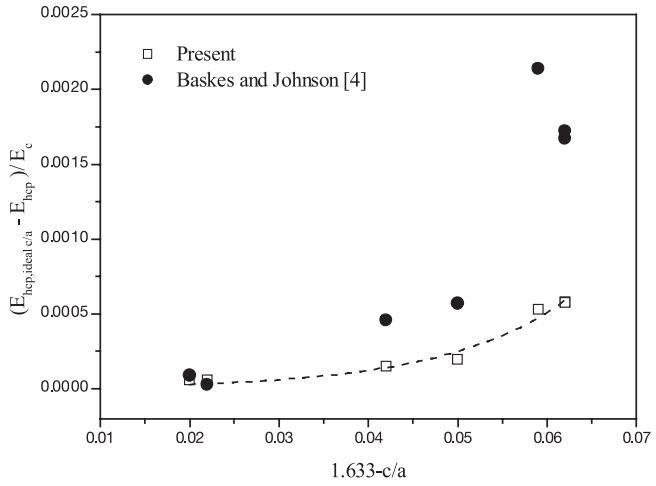

Fig. 6. Relation between the structural energy difference $(E_{\mathrm{hcp,\ idealc/a}} - E_{\mathrm{hcp}})/E_c$ and (1.633 - c/a).

3.3 Surface and stacking fault energy

Using the methodology of Ackland [12], the surface energy has been calculated and the results are summarized in Table 4. The calculated surface energies for the basal and prism planes are about equal, and their values are small as comparing with those from other models. B-J potentials [7] generally predicted a much high value of surface energy for these metals, and ranged from 885 to 2328 mJ/m^2 for different metals, great difference in surface energy for these rare earth metals. However, the calculations from Miedema's theory [18] and the present model indicate that the difference of surface energy of these metals is small, and Miedema's theory gave a somewhat higher value of surface energy than the present potentials. The surface tension near the melting point is also included in this table [23], the present results are closed to these experimental data. In general, the EAM or F-S potentials underestimated the surface energy, for example in bcc metals [24,25].

Using the present potentials, the stacking fault energies I_2, I_1 and E have been calculated and are summarized in Table 5. The present results are much lower than those from B-J potentials [7], in a similar way as surface energy. Attempts to adjust the potentials so as to achieve a high stacking fault energy were unsuccessful due to problems of lattice stability.

3.4 Vacancy and divacancy

The relaxed vacancy formation energy and formation volume have been calculated and are listed in Table 6 (The unrelaxed vacancy formation energy is shown in brackets). The difference of the vacancy formation energy between relaxed and unrelaxed values are very small, ranges from 0.016 to 0.034 eV, less than 3%. The formation volume is almost the same for these rare earth metals. The migration energy for a vacancy is the difference between the energy for an atom at the saddle point and that at its equilibrium site as it moves from its crystal site to the nearest vacant site. For hcp metals, there are two saddle points in this path, denoted as C and B_c respectively, which correspond to the migration of an atom out of the basal plane and in the basal plane. The present calculations for the migration energies E_{1m}^{out} and E_{1m}^{in}, and then the activation energy for self-diffusion $Q_{1v}^{out} = E_{1m}^{out} + E_{1f}$ (out of plane) and $Q_{1v}^{in} = E_{1m}^{in} + E_{1f}$ (in plane) are also shown in Table 6. In general, the self-diffusion energy of out-of-basal plane is not the same as that of in-basal plane. The isotropic nature of vacancy migration is observed for Ti and Co, and the migration in the basal plane is preferred for Mg, however, the migration in the out-of-plane is preferred for Zr, as reviewed by Bacon [4,5]. Another report for Zr is that the activation energy for self-diffusion to be independent of a change in the c/a ratio and the migration in the basal plane was preferred [26]. In the previous paper [14], we found that the isotropic nature of vacancy migration is observed for Mg and Co whose c/a ratio is close to the ideal value, and the migration in the out-of-plane is preferred for Be, Hf, Re, Ru, Sc, Ti, Y and Zr. It is the similar case for rare earth metals. The difference of activation energy for self-diffusion between basal plane and out-of-plane decreases almost linearly with increasing c/a ratio as shown in Figure 9.

The divacancy formation and binding energies of the first-nearest neighbors (FN) and the second-nearest neighbors (SN) configurations are calculated and listed in Table 7 (The data in brackets are unrelaxed values.) The unrelaxed binding energy of divacancy is almost the same as the relaxed one, and the value in the non-basal plane is somewhat smaller that in basal plane, which implies the divacancy was preferred to form in the basal plane. All of them are positive, indicating that these configurations are stable. However, the B-J potentials [7] predicted the divacancy is unbound for these metals.

Two configurations (FN and SN) for the migration of a divacancy are considered in a similar way as described in the previous paper [14]. The results are shown in Table 8. The diffusion activation energy difference for these configurations is not too large, all paths are possible for diffusion. The divacancy migration energy of j_2 or j_1 path is the lowest in FN or SN configuration, respectively, so j_2 or j_1 path may be the most favorable diffusion path for FN or SN configuration. Since FN transforms to SN after a j_2 jump and SN converts to FN after a j_1 jump, continuous migration can proceed with these two jumps.

3.5 Self-interstitial atoms

Self-interstitial atom (SIA) formation energy has been calculated for eight sites that have been suggested as possible interstitial positions by Johnson and Beeler [27]. The results are listed in Table 9, where the initial site and relaxed configuration are also shown. Note that some configurations are unstable and transform to a stable one. B_t transforms to B_c for all metals. T transforms to B_s or B_c. B_o is stable for Dy, Er, Ho and Pr, it transforms to B_c for

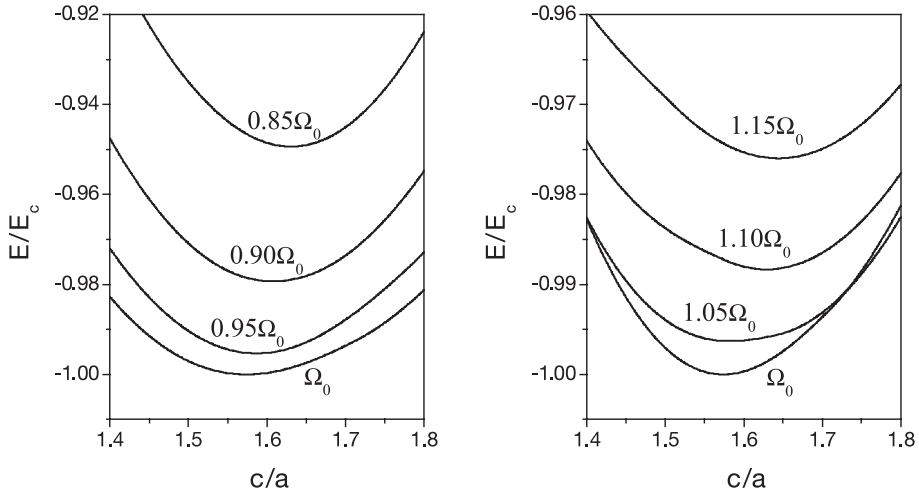

Fig. 7. Dependence of cohesive energy on c/a ratio at different values of the atomic volume for Dy.

Table 4. Calculated values of surface energy (mJ/m^2).

Element		Dy	Er	Gd	Ho	Nd	Pr	Tb
Basal	Present	519	583	487	538	515	486	519
plane	B-J [7]	2328	2318	1332	2180	1071	885	1515
Prism	Present	517	578	482	536	508	481	514
plane	B-J [7]	2238	2247	1286	2076	1150	945	1487
Miedema (average) [18]		1140	1170	1110	1150	1080	1080	1130
Gschneidner [23]		648	637	664	650	687	707	669

Table 5. Calculated values of the unrelaxed stacking fault energies (mJ/m^2).

Element	Dy	Er	Gd	Ho	Nd	Pr	Tb
I_2	26.2	32.2	19.9	32.8	23.0	26.0	19.4
I_1	13.1	16.1	9.9	16.4	11.5	13.0	9.7
E	39.3	48.3	29.8	49.2	34.5	39.0	29.1
B-J (I_2) [7]	168	160	84	156	32	22	92

Table 6. Predicted monvacancy properties. The data in parentheses are unrelaxed values. The c/a ratios are listed for referring.

Element	E_{1f} (eV)	E_{1m}^{out} (eV)	Q_{1v}^{out} (eV)	E_{1v}^{in} (eV)	Q_{1v}^{in} (eV)	$V_f(\omega_0)$	c/a
Dy	1.216 (1.237) 1.25 (1.34) [7]	0.629	1.845 (1.866)	0.708	1.924 (1.945)	0.854	1.574
Er	1.314 (1.339) 1.37 (1.45) [7]	0.660	1.974 (1.999)	0.742	2.056(2.081)	0.851	1.571
Gd	1.138 (1.154) 1.25 (1.25) [7]	0.636	1.774 (1.790)	0.693	1.831 (1.847)	0.802	1.591
Ho	1.266 (1.288) 1.34 (1.38) [7]	0.646	1.912 (1.934)	0.731	1.997 (2.019)	0.854	1.571
Nd	1.230 (1.258) 1.01 (1.00) [7]	0.536	1.766 (1.794)	0.552	1.782 (1.810)	0.829	1.613
Pr	1.231 (1.255) 0.92 (0.91) [7]	0.475	1.706 (1.730)	0.488	1.719 (1.743)	0.842	1.611
Tb	1.179 (1.203) 1.29 (1.27) [7]	0.612	1.791 (1.815)	0.680	1.859 (1.883)	0.813	11.583

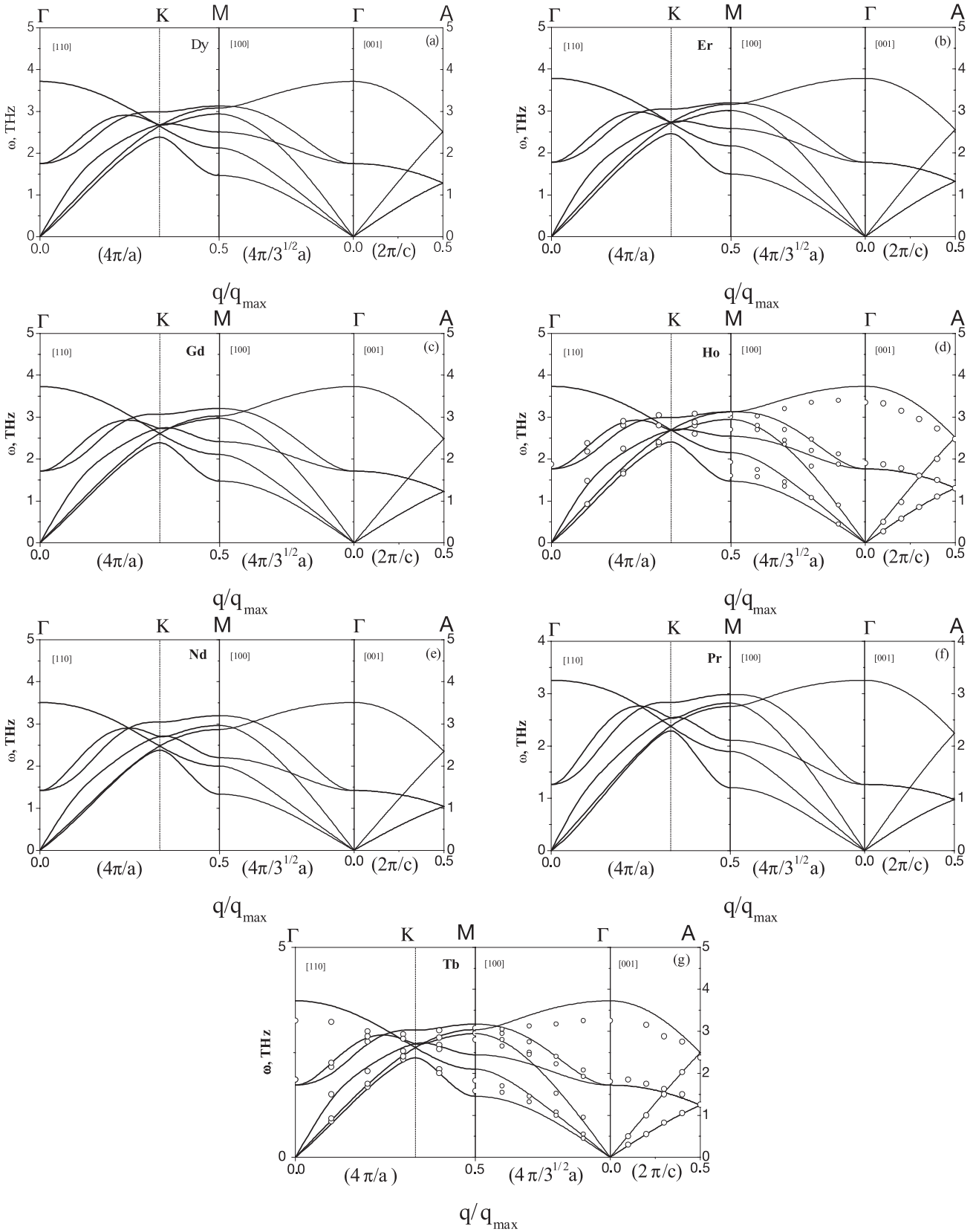

Fig. 8. Phonon dispersion relations for [110], [100] and [001] directions in the Brillouin zone of the hexagonal lattice for hcp rare earth metals. (a) Dy, (b) Er, (c) Gd, (d) Ho, (e) Nd, (f) Pr, and (g) Tb.

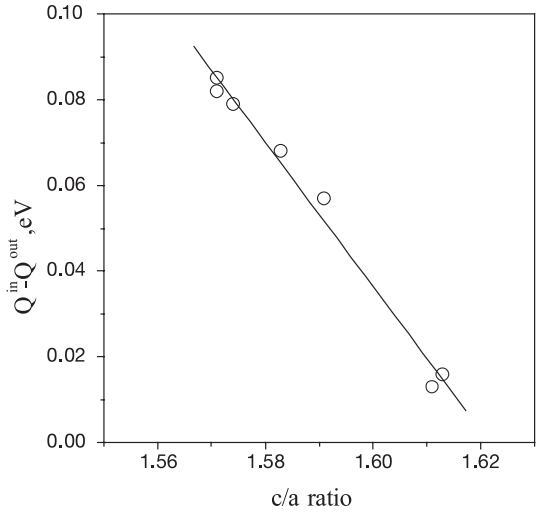

Fig. 9. Dependence of the difference of diffusion energy along basal and non-basal plane on c/a ratio.

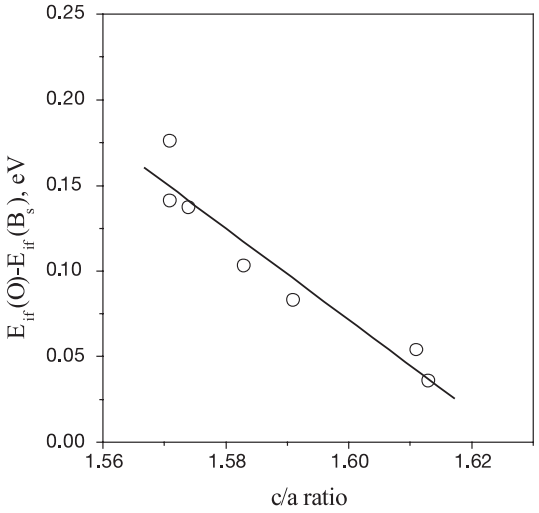

Fig. 10. Dependence of the difference of SIA formation energy between O and BS sites on c/a ratio.

Table 7. Calculated divacancy formation and binding energies (in eV/atom).

	FN (out of plane)			SN (in plane)		
Metals	Formation energy (eV)	Binding energy (eV)	Formation volume (Ω_0)	Formation energy (eV)	Binding energy (eV)	Formation volume (Ω_0)
Dy	2.269 (2.308)	0.163 (0.166)	1.718	2.258 (2.304)	0.174 (0.170)	1.699
		−0.66 [7]			−0.70 [7]	
Er	2.457 (2.502)	0.171 (0.176)	1.712	2.445 (2.497)	0.183 (0.181)	1.690
		−0.64 [7]			−0.68 [7]	
Gd	2.123 (2.160)	0.153 (0.148)	1.633	2.116 (2.157)	0.160 (0.151)	1.619
		−0.39 [7]			−0.31 [7]	
Ho	2.360 (2.399)	0.172 (0.177)	1.723	2.350 (2.395)	0.182 (0.181)	1.700
		−0.59 [7]			−0.63 [7]	
Nd	2.290 (2.348)	0.170 (0.168)	1.605	2.284 (2.345)	0.176 (0.171)	1.600
		−0.37 [7]			−0.38 [7]	
Pr	2.281 (2.330)	0.181 (0.180)	1.619	2.275 (2.328)	0.187 (0.182)	1.632
		−0.30 [7]			−0.31 [7]	
Tb	2.208 (2.253)	0.150 (0.153)	1.633	2.198 (2.249)	0.160 (0.157)	1.618
		−0.44 [7]			−0.47 [7]	

other metals. C and S transform to B_s for Er and Ho, and to form a dumbbell for others. B_c, B_s and O are the stable configurations for these metals. The formation energy of B_s or B_c is the lowest, thus, the most stable SIAs are B_c and B_s. On the other hand, the formation energy of O is the largest. The difference of the formation energy between site O and B_s is small (the maximum is 0.176 eV for Er), and it decreases linearly with increasing c/a ratio as shown in Figure 10, a similar case as the vacancy diffusion energy difference between basal and non-basal plane.

The lowest formation energy of SIA for these metals is plotted against kT_m in Figure 11. The formation energy increases linearly as melting temperature increasing. This gives a relationship between SIA formation energy and kT_m, *i.e.*, $E_{if} = 22.9kT_m$. Bacon [5] suggested that the reasonable value of formation energy of SIA should fall in the range of $18 - 25kT_m$ from the calculations with the pair and many-body potentials. The formation volume of SIA in the eight configurations is also presented in Table 9. The contribution from the relaxation volume varies considerably from metal to metal.

4 Conclusions

(1) The EAM-type many-body potentials for seven hexagonal close-packed rare earth metals are constructed.
(2) Calculations of the mechanical stability of the corresponding hcp lattice with respect to large changes of

Table 8. Divacancy migration and diffusion activation energies (in eV/atom).

		Dy	Er	Gd	Ho	Nd	Pr	Tb
E_{j1}^{FN}		0.621	0.654	0.602	0.648	0.509	0.480	0.591
E_{j2}^{FN}		0.508	0.537	0.503	0.527	0.415	0.380	0.486
E_{j3}^{FN}		0.879	0.924	0.849	0.911	0.727	0.669	0.843
E_{j4}^{FN}		0.769	0.807	0.768	0.794	0.684	0.626	0.749
E_{j5}^{FN}		0.833	0.874	0.813	0.861	0.687	0.622	0.804
E_{j6}^{FN}		0.735	0.772	0.739	0.757	0.650	0.588	0.718
Q_{2v}^{FN}	Min.	2.777	2.994	2.626	2.887	2.705	2.661	2.694
	Max.	3.148	3.381	2.972	3.271	3.017	2.950	3.051
E_{j1}^{SN}		0.510	0.539	0.504	0.528	0.416	0.381	0.487
E_{j2}^{SN}		0.692	0.728	0.657	0.723	0.530	0.497	0.653
E_{j3}^{SN}		0.793	0.833	0.789	0.819	0.709	0.656	0.771
E_{j4}^{SN}		0.750	0.786	0.753	0.772	0.669	0.607	0.732
E_{j5}^{SN}		0.830	0.870	0.811	0.858	0.686	0.621	0.801
E_{j6}^{SN}		0.806	0.846	0.787	0.833	0.658	0.593	0.777
Q_{2v}^{SN}	Min.	2.768	2.984	2.620	2.878	2.700	2.656	2.685
	Max.	3.088	3.315	2.927	3.208	2.970	2.896	2.999

Table 9. Calculated formation energies and volumes for self-interstitial atom at different positions.

Initial position	Element	Dy	Er	Gd	Ho	Nd	Pr	Tb
B_C	E_{if} (eV)	3.287	3.462	3.309	3.344	2.665	2.204	3.222
	$V_{if}(\Omega_0)$	1.188	0.969	1.555	1.118	1.130	0.681	1.398
	Final position	B_C	B_C	B_C	B_C	B_C	B_C	B_C
B_O	E_{if} (eV)	3.421	3.567	3.309	3.467	2.665	2.251	3.222
	$V_{if}(\Omega_0)$	1.251	1.020	1.548	1.184	1.116	0.815	1.397
	Final position	B_o	B_o	B_C	B_o	B_C	B_o	B_C
B_S	E_{if} (eV)	3.286	3.459	3.309	3.343	2.665	2.204	3.222
	$V_{if}(\Omega_0)$	1.162	0.981	1.564	1.118	1.143	0.734	1.400
	Final position	B_S	B_S	B_S	B_S	B_S	B_S	B_S
B_T	E_{if} (eV)	3.287	3.462	3.309	3.344	2.665	2.204	3.222
	$V_{if}(\Omega_0)$	1.190	0.995	1.558	1.117	1.159	0.755	1.401
	Final position	B_C	B_C	B_C	B_C	B_C	B_C	B_C
C	E_{if} (eV)	3.368	3.459	3.363	3.343	2.688	2.238	3.288
	$V_{if}(\Omega_0)$	1.293	0.953	1.656	1.098	1.212	0.743	1.488
	Final position	Dumb	B_S	Dumb	B_S	Dumb	Dumb	Dumb
O	E_{if} (eV)	3.423	3.635	3.392	3.483	2.701	2.258	3.325
	$V_{if}(\Omega_0)$	1.355	1.111	1.760	1.304	1.208	0.767	1.588
	Final position	O	O	O	O	O	O	O
S	E_{if} (eV)	3.367	3.459	3.363	3.343	2.689	2.237	3.291
	$V_{if}(\Omega_0)$	1.248	0.930	1.658	1.090	1.241	0.750	1.517
	Final position	Dumb	B_S	Dumb	B_S	Dumb	Dumb	Dumb
T	E_{if} (eV)	3.287	3.462	3.309	3.343	2.665	2.204	3.222
	$V_{if}(\Omega_0)$	1.176	0.983	1.553	1.100	1.126	0.736	1.403
	Final position	B_C	B_C	B_C	B_S	B_C	B_S	B_C

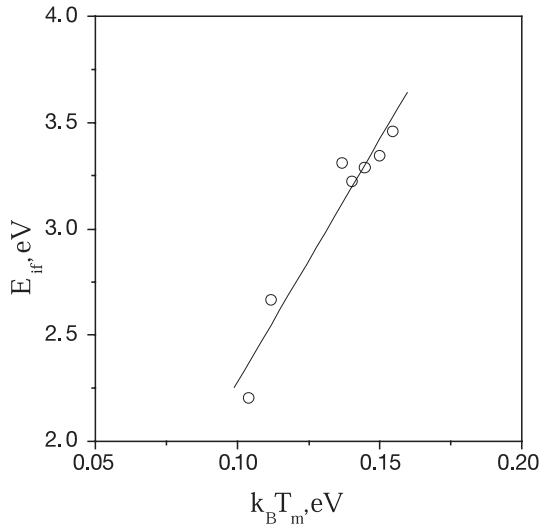

Fig. 11. Relation between self-interstitial atom formation energy and melting temperature.

density and c/a ratio, and the structural stability of the real hexagonal close-packed lattice relative to fcc, bcc as well as the hcp structure with the ideal c/a ratio shows that the fitted hcp lattice is the most stable structure.

(3) Phonon dispersion curves were calculated for the [100], [110] and [111] directions. They were in good agreement with experimental data available.

(4) The calculated surface and stacking fault energies are rather low as comparing with those from B-J potentials.

(5) The activation energies for self-diffusion by mono-vacancies and di-vacancies are calculated. j_2 and j_1 were the most favorable diffusion paths for the FN and SN configuration, respectively, and a continuous diffusion path could be formed with these two jumps.

(6) Formation energies and volumes were obtained for various interstitial configurations. B_c and B_s are the most stable configurations. The SIA formation energy increases linearly with increasing of the melting temperature and it gives $E_{if} = 22.9kT_m$.

W. Hu thanks the award of a Fellowship through the Japan Society for the Promotion of Science for an extended visit to Toyohashi University of Technology. This research was supported by the Ministry of Education of China.

References

1. C. Domain, C.S. Becquart, Phys. Rev. B **65**, 024103 (2001)
2. S. Han, L.A. Zepeda-Ruiz, G.J. Ackland, R. Car, D.J. Srolovitz, Phys. Rev. B **66**, 220120 (2002)
3. S. Han, L.A. Zepeda-Ruiz, G.J. Ackland, R. Car, D.J. Srolovitz, J. Appl. Phys. **93**, 3328 (2003)
4. D.J. Bacon, J. Nucl. Mater. **159**, 176 (1988)
5. D.J. Bacon, J. Nucl. Mater. **249**, 206 (1993)
6. M. Igarashi, M. Khantha, V. Vitek, Philos. Mag. B **63**, 603 (1991)
7. M.I. Baskes, R.A. Johnson, Modelling Simul. Mater. Sci. Eng. **2**, 147 (1994)
8. D.J. Oh, R.A. Johnson, J. Mater. Res. **3**, 471 (1988)
9. R.A. Johnson, D.J. Oh, J. Mater. Res. **4**, 1195 (1989)
10. R.A. Johnson, Philos. Mag. A **63**, 865 (1991)
11. G.J. Ackland, Philos. Mag. A **66**, 917 (1992)
12. G.J. Ackland, S.J. Wooding, D.J. Bacon, Philos. Mag. A **71**, 553 (1995)
13. W. Hu, H. Xu, X. Shu, X. Yuan, B. Gao, B. Zhang, J. Phys. D: Appl. Phys. **33**, 711 (2000)
14. W. Hu, B. Zhang, B. Huang, F. Gao, D.J. Bacon, J. Phys.: Cond. Matt. **13**, 1193 (2001)
15. W. Hu, M. Fukumoto, Modelling Simul. Mater. Sci. Eng. **10**, 707 (2002)
16. C.S. Barrett, T.B. Massalski, *Structure of Metals*, 3rd edn. (Pergamon Press, 1980), p. 626
17. C. Kittel, *Introduction to Solid State Physics* (Wiley, New York, 1976), p. 74
18. F.R. de Boer, R. Boom, W.C.M. Mattens, A.R. Miedema, A.K. Nissen, *Cohesion in Metals: Transition Metal Alloys* (Amsterdam, North-Holland, 1988)
19. *Smithells Metal Reference Book*, 7th edited by E.A. Brandes, G.B. Brook, (Oxford, Butterworths, 1992), p. 15–16
20. J.H. Rose, J.R. Smith, F. Guinea, J. Ferrante, Phys. Rev. B **29**, 2963 (1984)
21. N. Singh, Physica B **203**, 22 (1994)
22. M. Born, K. Huang, *Dynamical Theory of Crystal Lattice* (Clarendon, Oxford, 1954)
23. K.A. Gschneidner Jr., *CRC Handbook of Chemistry and Physics*, edited by D.R. Lide, 83rd edn (CRC Press 2002), pp. 4–130
24. M.W. Finnis, J.E. Sinclair, Philos. Mag. A **50**, 45 (1984)
25. A.M. Guellil, J.B. Adams, J. Mater. Res. **7**, 639 (1992)
26. D.J. Oh, R.A. Johnson, J. Nucl. Mater. **169**, 5 (1989)
27. R.A. Johnson, J.R. Beeler, Jr., *Interatomic Potentials and Crystalline Defects*, edited by J.K. Lee (Warrendale, PA, 1981), p. 165